RSC Advances

ROYAL SOCIETY OF CHEMISTRY

www.rsc.org/advances

Cite this: DOI: 10.1039/c0xx00000x

www.rsc.org/xxxxxx

ARTICLE TYPE

Synthesis of a novel tunnel $Na_{0.5}K_{0.1}MnO_2$ composite as cathode for sodium ion batteries

Zhen-guo Wu,[a,b] Yan-jun Zhong,[b] Jun-tao Li, *[a] Kai Wang,[b] Xiao-dong Guo, *[b] Ling Huang,[c] Ben-he Zhong,[b] and Shi-gang Sun[a,c]

Received (in XXX, XXX) Xth XXXXXXXXX 20XX, Accepted Xth XXXXXXXXX 20XX

DOI: 10.1039/b000000x

A novel tunnel $Na_{0.5}K_{0.1}MnO_2$ composite assembled by two different tunnel structures of $Na_{0.44}MnO_2$ and KMn_8O_{16} is synthesized by co-precipitation method. Bundles of microrods and small nanorods could be observed in $Na_{0.5}K_{0.1}MnO_2$ composite. The composite possesses highly crystallinity and large stacking faults. When used as cathode for sodium ion batteries, the composite exhibits high specific capacity, excellent cycleability and superior rate capability. A high reversible discharge capacity of 142.3 mAh g^{-1} could be delivered at 0.1 C, with 94.7 mAh g^{-1} retained after 100 cycles. And 82.2 mAh g^{-1} could be maintained after 300 cycles at 1.0 C. More than 70 mAh g^{-1} could be obtained at a high rate of 4.0 C. The outstanding electrochemical performances may be attributed to the combined tunnel structures, one-dimensional rod-like morphology and massive structural stacking faults.

1. Introduction

In the past decades, a great development of lithium ion batteries (LIBs) has been achieved with huge efforts of numerous researchers. And lithium ion batteries have dominated the field of electronic equipment, as well as the successful application in hybrid electrical vehicles (HEVs), electrical vehicles (EVs) and energy storage stations.[1-3] However, the limited natural lithium reserves and relative high cost may severely hinder the application of LIBs in large-scale renewable energy storage. Sodium ion batteries (SIBs), with the advantages of chemical similarities with LIBs, natural abundance, evenly distribution of sodium reserves and low toxicity, have been regarded as feasible alternative technology. [4-9]

Various cathode materials for SIBs have been developed, including layered oxides,[10-12] polyanionic compouds[13-15] and other oxides.[16, 17] Manganese (Mn) based oxides have been recognized as one of the prominent cathodes due to their attractive features of natural abundance, low-cost and non-toxicity.[18] Among the Mn based oxides, tunnel $Na_{0.44}MnO_2$, with some outstanding properties such as relative high capacity, good cycling stability, reversible cyclability in aqueous electrolyte[19] and excellent rate capability, has attracted much attentions.[20-26] Some pioneer works with encouraging results about tunnel $Na_{0.44}MnO_2$have been done. Sauvage et al. synthesized pure $Na_{0.44}MnO_2$ via a solid state reaction method, with an initial capacity of 80 mAh g^{-1} at 1/10 C rate between 2.0-3.8 V (vs. Na/Na^+).[22] Cao and his coworkers prepared $Na_{0.44}MnO_2$ nanowires and demonstrated that the controlled structure could obviously enhance the electrochemical properties.[26] The $Na_{0.44}MnO_2$ nanowires electrode delivered 128 mAh g^{-1} at 12 mA g^{-1} with outstanding cyclability between 2.0-4.0 V (vs. Na/Na^+). Nevertheless, the nanowire was obtained by a polymer-pyrolysis method, which is complicated and expensive. Some other researches had also proved the prominent application of $Na_{0.44}MnO_2$ material in SIBs.[20, 27, 28] But it's still challenging to produce $Na_{0.44}MnO_2$ material with high capacity and excellent cycling stability through a cost effective method. Meanwhile, it's noticeable that some previous reports have indicated that the cryptomelane-type KMn_8O_{16} with tunnel structure could be a suitable cathode for LIBs.[29, 30] The KMn_8O_{16} microclusters assembled by nanofiber also showed reversible high reversible capacity of 360 mAh g^{-1} at 100 mA g^{-1} and good cycling stability.[30] What's more, the superior cyclability of KMn_8O_{16} with wide voltage range of 1.5-4.2 V indicate a high structural stability. Considering the similarities between Na ion and Li ion, excellent electrochemical performances of KMn_8O_{16} in SIBs could be expected. Recently, the great research results about layer-spinel cathode materials[31-33] in LIBs show the effectvie strategy to enhance the electrochemcial performances by introducing the interaction between different structures. Based on these review, an attempt to combine the two tunnel structures could be carried out.

Here, we synthesized rod-like $Na_{0.5}K_{0.1}MnO_2$ composite by a simple co-precipitation method. The $Na_{0.5}K_{0.1}MnO_2$ composite is composed of two different tunnel structures ($Na_{0.44}MnO_2$ and KMn_8O_{16}). A high reversible capacity of 144.7 mAh g^{-1} is delivered at 0.1 C, with 94.7 mAh g^{-1} retained after 100 cycles. And 82.2 mAh g^{-1} could be maintained at 1.0 C after 300 cycles. More than 70 mAh g^{-1} could be obtained at a high current density of 4.0 C. The results demonstrate that the composite possesses high capacity, excellent cycling performance and superior rate capability.

2. Experimental

2.1 2.1 Preparation of $Na_{0.5}K_{0.1}MnO_2$

$Na_{0.5}K_{0.1}MnO_2$ composite was synthesized by co-precipitation method. Typically, analytical reagent grade $NaCH_3COO•3H_2O$, KCH_3COO and $Mn(CH_3COO)_2•3H_2O$ in a molar ratio of 0.5:0.1:1 and in quantities corresponding to 0.05 mol of the target $Na_{0.5}K_{0.1}MnO_2$ were dissolved in 100 ml of deionized water. 12.61 g of $H_2C_2O_4•2H_2O$, which was dissolved in another cup of

100 ml of deionized water, was added to the mixed solution of K, Na, Mn acetate. Then, the water was evaporated at 80 ℃ to afford a milky white precursor. After dried at 80 ℃ overnight, the precursor was pressed into pellets and preliminaries annealed at 450 ℃ for 6 h with subsequent heat treatment of 800 ℃ 15 h. Finally, the pellet was quenched to room temperature in liquid nitrogen and stored in the glove box with Ar atmosphere.

2.2 Characterization and electrochemical measurements

The Chmical composition of the sample was determined by using an inductively coupled plasma-optical emission spectrometer (ICP-OES, Thermo Electron IRIS Intrepid II XSP). Thermogravimetric analysis was performed on a simultaneous thermal analysis apparatus (SDT Q600, TA instrument). The morphology and structure of the as-prepared sample were characterized by field emission scanning electron microscopy (SEM, HITACHI S-4800), transmission electron microscopy (TEM, JEM 2100), Raman system (Xplora, Horiba), and powder X-ray diffraction (XRD, Philips X'pert Pro Super X-ray diffract meter, Cu Kα radiation) measurements. X-ray photoelectron spectroscopy (XPS) experiments were carried out on a PHI QUANTUM 2000 instrument. Electrodes of sodium half-cell were made by spreading a mixture of 80 wt % $Na_{0.5}K_{0.1}MnO_2$ active material, 10 wt % acetylene black and 10 wt % PVDF onto aluminum foil current collectors. The mass loading of the active materials is 2.0 mg cm^{-2}. The as-prepared electrodes were dried at 80 °C in a vacuum oven for 12 h. Electrochemical properties of the electrodes were monitored by assembling them into coin cells (type CR2025) in an argon-filled glove box with water and oxygen contents less than 5 ppm. Metallic Na was used as the counter electrode and glass fiber (GF/A, Whatman) as separator. The electrolyte was made of $NaClO_4$ (1 mol L^{-1}) and a mixture of PC/EC in a volume ratio of 1:1 (purchased from Fosai New Materials Co., Ltd., Jiangsu, China). The cells were galvanostatically charged and discharged on a battery test system (LAND-2001A, Land Electronic Co., Ltd., Wuhan, China) with a cut-off voltage range of 1.5-4.3 V (*vs.* Na/Na^+). Cyclic voltammetry (CV) was conducted on a CHI 660D electrochemical workstation (CH Instruments Co., Ltd., Shanghai, China) using coin cell at a scan rate of 0.2 mV s^{-1} with the same cut-off voltage range for electrochemical tests were conducted at 30°C. The cells charged/discharged to a certain voltage were disassembled in glove box. and the active material electrodes were taken out, washed with dimethyl carbonate and dried. The ex-situ XRD patterns were also collected on Philips X'pert Pro Super X-ray diffract meter.

3. Results and Discussion

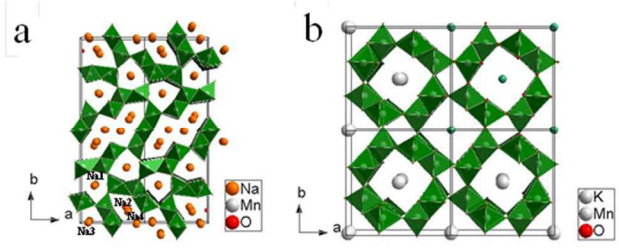

Figure1. Schematic crystal structures of $Na_4Mn_9O_{18}$ (a) and KMn_8O_{16} (b).

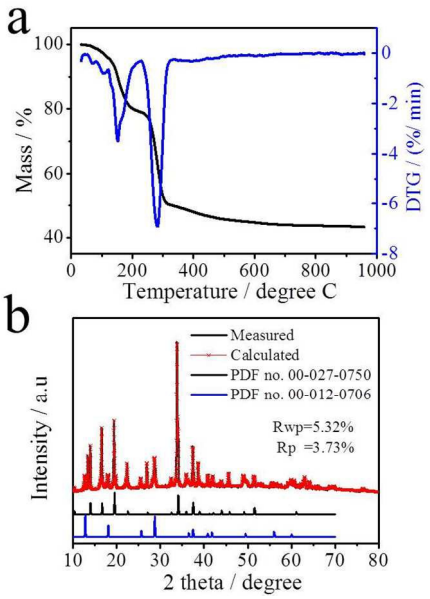

Figure2. TG and DTG curves of precursor (a) and Rietveld refinement of XRD patterns of $Na_{0.5}K_{0.1}MnO_2$.

The crystal structure of tunnel $Na_{0.44}MnO_2$ with space group of *Pbam* is shown in Fig.1a. Four MnO_6 octahedral sites and one MnO_5 square-pyramidal site construct the framework structure of $Na_{0.44}MnO_2$. And a double-tunnel structure is built up from double and triple chains of MnO_6 octahedral and single chains of MnO_5 square-pyramids by either edge or corner sharing. Four crystallographically distinct Na^+ sites exist within the tunnel of $Na_{0.44}MnO_2$. Na1 locates in the six-sided tunnel, while the others (Na2, Na3 and Na4) reside in the large S-shaped tunnel (Fig.1a). Sodium ions in large tunnels are highly mobile.[23, 34] The unique large and double tunnel structure can also help to tolerate structural strains during charge-discharge processes, which can offer outperformed cyclability. The Cryptomelane KMn_8O_{16} shows an I4/m tetragonal structure with a distinct tunnel feature. The frame structure of KMn_8O_{16} is built up by double chains of edge-sharing MnO_6 octahedral, forming tunnel structures, with K ions situated in the large tunnels (Fig.1b). The K ions can not only maintain the structure, but also increase the ion diffusion rate.[35]

Fig.2a shows TG/DTG curves of precursor at a heating rate of 10 ℃/min from room temperature to 1000 ℃ under air. The weight loss before 150 ℃ is attributed to the dehydration of the precursor. And further thermal decomposition occurred at around 300 ℃. The final weight loss between 300 and 700 ℃ may be ascribed to the crystallization of the product. No obvious weight loss could be found after 700 ℃. According to the results, the pre-calcination was carried out at 450 ℃ for 6 h to guarantee the complete thermal decomposition of the precursor. And further heat treatment at 800 ℃ for 15 h was applied to enhance the crystallinity of the final product. The molar ratio of Na, K, Mn is 0.498:1.003:1, which is close to the feed ratio of raw materials.

Rietveld refinement result of XRD pattern with PDXL program of $Na_{0.5}K_{0.1}MnO_2$ is given in Fig.2b. Most of the diffraction peaks can be indexed to orthorhombic $Na_{0.44}MnO_2$ (PDF no. 00-027-0750) and tetragonal KMn_8O_{16} (PDF no. 00-012-0706). And no obvious impurity could be found. The lattice constants of

$Na_{0.44}MnO_2$ are a=9.092 Å, b=26.505 Å, c=2.827 Å, which are in accord with previous reports.[20, 36, 37] the lattice parameter of KMn_8O_{16} are a=b=9.914 Å, c=3.194 Å. The mass ratio of $Na_{0.44}MnO_2$ and KMn_8O_{16} is 86.6%:13.4%.

Fig.3 displays the high resolution XPS spectra of $Na_{0.5}K_{0.1}MnO_2$. As shown in Fig.3a, in addition to the C 1s level observed at 284.8 ev, two strong peaks appear at higher binding energy (>290 ev), which could be assigned to K $2p_{3/2}$ and $2p_{1/2}$. The observation of spin-orbital levels gives a direct evidence for the existence of potassium in $Na_{0.5}K_{0.1}MnO_2$ composite.[38] Mn 2p spectra with Gaussian fitting result indicates that energies centered at 641.9 ev, 640.5 ev, 653.7 ev and 652.4 ev could be ascribed to the presence of tetravalent Mn and trivalent Mn, which is agree with the crystal structure and some previous reports.[39-41]

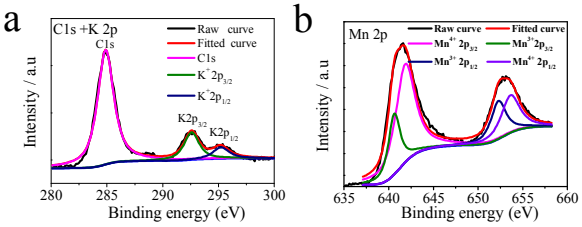

Figure 3. High resolution XPS spectra with Gaussian Fitting for C 1s and K 2p peaks (a) and Mn 2p (b).

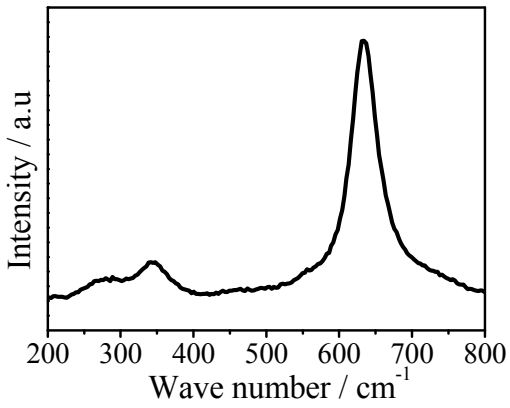

Figure 4. Raman spectra of $Na_{0.5}K_{0.1}MnO_2$

Further structural information was obtained by Raman measurement with a 532 nm lasers as the excitation light (Fig.4). The spectral shape and peaks locations are consistent with the previous reports, which confirm the existence of orthorhombic $Na_{0.44}MnO_2$.[20] Band at ~640 cm^{-1} maybe assigned to stretching vibrations of Mn-O, while the band at ~360 cm^{-1} is due to the bend vibrations of O-Mn-O.[20, 42]

Particles with two different morphologies could be observed in $Na_{0.5}K_{0.1}MnO_2$ composite (Fig.5a). The large rod-like bundles assembled by microrods with a width of ~200 nm and ~10 μm in length could be identified (Fig.5a and 5b), which could be attributed to sinter at high temperature.[20] Meanwhile, small nanorods with a diameter of 50 nm and a length of 500 nm were also clearly investigated (Fig.5c). Large stacking faults could be detected in the microrods (Fig.5d), which could be related to the introduction of KMn_8O_{16} and maybe enhance the electrochemical

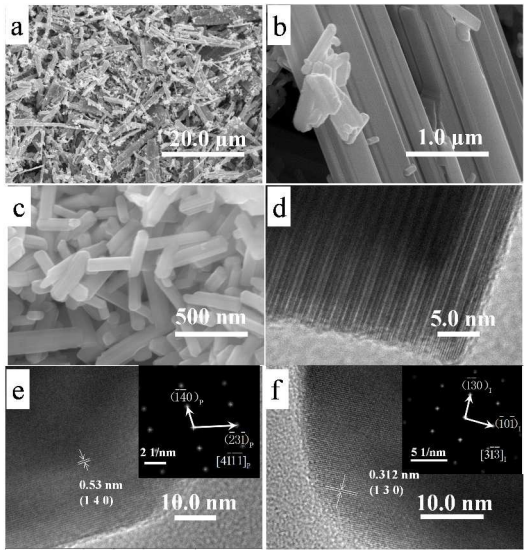

Figure 5. SEM images (a, b, c). TEM image (d), HRTEM images (e, f) and SAED patterns (inset e, f) of $Na_{0.5}K_{0.1}MnO_2$

performance.[43] Lattice fringes in the HRTEM image (Fig.5e) of the microrods are ~0.53 nm, corresponding to the interplanar distance of the (1 4 0) plane in $Na_{0.44}MnO_2$. The lattcie fringes of ~0.312 nm in small nanorods (Fig.5f) can be ascribed to the (1 3 0) plane in KMn_8O_{16}. The Fast Fourier Transformation (FFT) results furtherly demonstrate the existence of $Na_4Mn_9O_{18}$ with orthorhomic lattice structure (*Pbam* space group) and KMn_8O_{16} with tetragonal structure (*I4/m* space group). The characterization of morphology furtherly demonstrate that the tunnel $Na_{0.5}K_{0.1}MnO_2$ is composed of two kinds of particles with separately orthorhomic or tetragonal structure, which could be related to the big differences between the two structures.

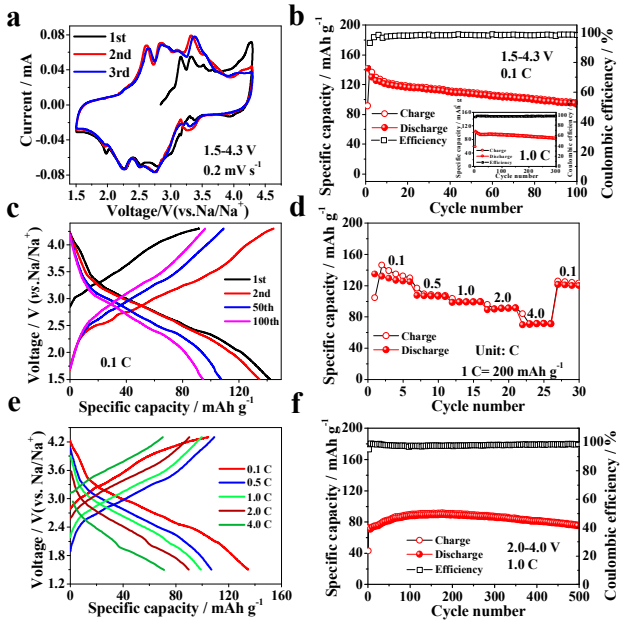

Figure 6. Electrochemical characterization and battery performance of $Na_{0.5}K_{0.1}MnO_2$: cyclic voltammetry curves (a); cycling performances at 0.1 C and 1C (b); typical charge-discharge curves between 1.5-4.3 V at 0.1 C(c); rate capability (d); representative charge-discharge curves at different C rates (e); cycling performance at 1.0 C between 2.0-4.0 V (f).

Fig.6a shows cyclic voltammetry plots of $Na_{0.5}K_{0.1}MnO_2$ composite at a scan rate of 0.2 mV s^{-1} between 1.50-4.30 V. Some differences could be found between the first cycle and the subsequent cycles. The oxidation peaks located at 3.16 V and 4.30 V are much stronger than that of the subsequent processes, which indicate some degree of irreversible reactions. The initial irreversible processes could be attributed to the multiatomic transition processes to relieve the structural strain for Na ion insertion-extraction and the surface reaction between the electrolyte and electrode. However, another two oxidation peaks between 3.24-3.60 V became stronger in the following cycles, which due to the activation process of KMn_8O_{16} in the first cycle.[29] After the first scan, the consequent CV curves display several pairs of symmetrical redox peaks, denoting the complex biphasic transition mechanism during charge-discharge process that had not been clearly identified. It is considered that the presence of multi-phase states is strongly related with Na^+/vacancy ordering, which is shown in Fig.1.[20, 44] It is interesting that the tunnel structure $Na_{0.5}K_{0.1}MnO_2$ material possesses relatively fewer redox peaks than normal $Na_{0.44}MnO_2$,[27] which could indicate that the introduction of KMn_8O_{16} would smoothen the CV curves.

Fig.6b demonstrated the excellent electrochemical performances of $Na_{0.5}K_{0.1}MnO_2$ with the cut-off voltage window of 1.5-4.3 V. A high reversible capacity of 142.3 mAh g^{-1} could be delivered at 0.1 C (20 mA g^{-1}), which is the highest result to the best of our knowledge. The high capacity could be ascribed to the existence of KMn_8O_{16} and the stacking faults, which provide more accessible sites of Na ions.[30] The composite also performed outstanding cycling stability, with 94.7 mAh g^{-1} maintained after 100 cycles. The coulombic efficiency reached 93% during the second cycle and further increased to >98% after 10 cycles. When cycled at 1 C (200 mA g^{-1}), 104.2 mAh g^{-1} was showed and 82.2 mAh g^{-1} was retained after a long-term cycling of 300 cycles. The representative charge-discharge curves at 0.1 C were arrayed in Fig.6c. In the initial cycle, the discharge capacity is much higher than the charge capacity, which is consistent with the CV results, indicates more Na ions could be stored in the orthorhombic lattice,[44] and shows the activation process of K-Mn_8O_{16}.[29] Some short voltage plateaus were observed in the successive charge-discharge curves, which could be assigned to the symmetrical redox peaks as shown in CV profiles. It also can be observed that the $Na_{0.5}K_{0.1}MnO_2$ composite showed much smoother charge-discharge curves in comparison with previous reports,[20] which is also in accord with CV results. What's more, the $Na_{0.5}K_{0.1}MnO_2$ composite possesses not only high reversible capacity and excellent cycling stability, but also good rate capability (Fig.6d). The test was started from 0.1 C and successively increased to 0.5 C, 1.0 C, 2.0 C and 4.0 C. And the respectively average capacities are 129.4 mAh g^{-1}, 106.7 mAh g^{-1}, 98.9 mAh g^{-1}, 89.9 mAh g^{-1} and 71.1 mAh g^{-1}. When the current density is back to 0.1 C, more than 120 mAh g^{-1} could be recovered, which demonstrated high reversibility. The selected charge-discharge curves at different C rates are shown in Fig.6e. The voltage plateaus could be detected even at 4.0 C, which demonstrate small electrode polarization. The outperformed rate capability is superior or at least comparable to the previous reports of $Na_{0.44}MnO_2$ and other tunnel structure composite,[20, 26] which may be attributed to the fast diffusivity of Na ions in the novel tunnel structure of $Na_{0.44}MnO_2$ and KMn_8O_{16}, as well as the one-dimensional morphology including microrods and nanorods. The results could also demonstrate that the K ions in the tunnel structure could increase the Na ion diffusion rate. In order to compare with some previous reports, the cycling performance between 2.0-4.0 V was also conducted. As shown in Fig.6f, a discharge capacity of 75 mAh g^{-1} was observed after 500 cycles at 1.0 C. The capacity increment phenomenon is maybe caused by the slow activation process in the narrow voltage range. And the cycling performance presented here is also at least comparable with previous reports.[20, 26] The enhanced electrochemical performances could be related to the highly crystalline structure, suitable particles size and incorporation of KMn_8O_{16}. The highly crystalline structure and coexistence of KMn_8O_{16} could lead to reversible phase transition during charge-discharge process and help maintain the structure stability in a relatively wide voltage range of 1.5-4.3 V. The rod-like morphology could effectively accommodate the structure strain during repeated Na ion insertion and extraction process. What's more, the one dimensional rods and K ions in the tunnel structure of KMn_8O_{16} could also facilitate the diffusion of Na ions.

In order to analyze the structural evolution during the Na ion insertion and extraction process, the ex-situ XRD measurement in the different charge-discharge stages at 0.1 C were carried out as shown in Fig.7. It is hard to clearly identify the appearance of a new phase, which is in accord with the results of Sauvage et al and Cao et al. Unlike previous reports of $Na_{0.44}MnO_2$, The (3 5 0) reflection is split into (3 5 0) and (0 10 0) in the pristine XRD pattern, which is in accord with the study result of Chu.et al. The portion of the (0 10 0) changed at different charge-discharge stages, which could be attributed to the evolution of the cell parameters. What's more, the location of diffraction lines belonged to KMn_8O_{16} kept unchanged during the charge-discharge process, which indicates high structure stability. The ex-situ XRD results indicate that different intermediate structures during complex phase transitions in the respectively charge-discharge stages are closely related, demonstrating a biphasic transition Na ion insertion-extraction mechanism. However, the detailed influence of incorporation of KMn_8O_{16} still needs more investigation.

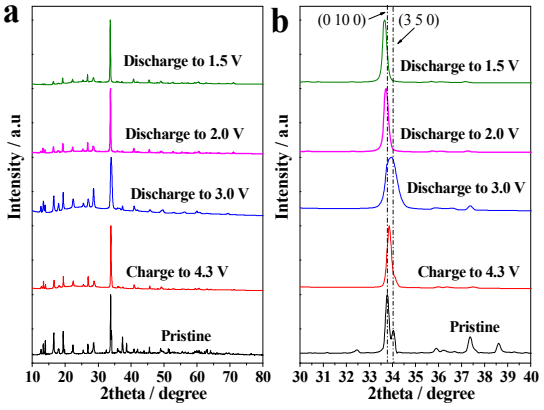

Figure 7. Ex-situ XRD patterns of $Na_{0.5}K_{0.1}MnO_2$ with the voltage range of 1.5-4.3 V in the first charge-discharge process.

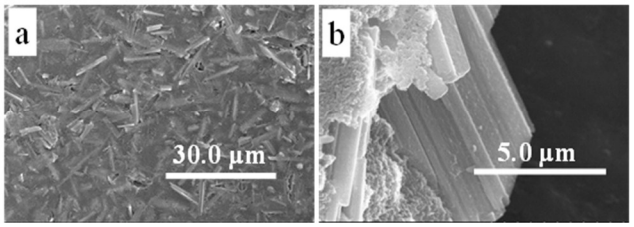

Figure 8. Morphology of electrode after 300 cycles at 1.0 C.

Morphology change of the electrode after 300 cycles at 1.0 C is presented in Fig.8a. No cracks appeared on the electrode, which indicate excellent mechanical stability. The rod-like morphology could be preserved after 300 cycles at 1.0 C, demonstrating high structural stability.

4. Conclusions

In summary, a novel composite $Na_{0.5}K_{0.1}MnO_2$composed of orthorhombic $Na_{0.44}MnO_2$ and tetragonal KMn_8O_{16} was prepared by co-precipitation method. Both of two phases contain large tunnel structure, which is beneficial for the insertion-extraction and diffusion of Na ions. The one-dimensional rod-like morphology and suitable particle size also help enhance the electrochemical performances in SIBs as cathode. The novel composite possesses high capacity, excellent capability and outperformed rate capability. A high reversible capacity of 142.3 mAh g^{-1} could be delivered at 0.1 C, with 94.7 mAh g^{-1} retained after 100 cycles between 1.5-4.3 V. The material could still deliver more than 70 mAh g^{-1} at 4.0 C. When cycled between 2.0-4.0 V, a discharge capacity of 75 mAh g^{-1} was observed after 500 cycles at 1.0 C. The Ex-situ results demonstrate the high structure stability of $Na_{0.44}MnO_2$ and KMn_8O_{16}. The results indicate that the composite could be prominent cathode for SIBs used in large-scale energy storage. And the study also proved a possible strategy to enhance the electrochemical performances of SIBs' cathode material by combining different structures.

Notes and references

[a] *college of energy, Xiamen University, Xiamen,361005 (PR China)*
[b] *School of Chemical Engineering, Sichuan University, Chengdu,610065 (PR China); E-mail:nic1201@163.com*
[c] *College of Chemistry and Chemical Engineering, Xiamen University, Xiamen,361005 (PR China)*

Acknowledgements
This work was supported by National Natural Science Foundation of China (21373008, 21321062 and 21273184) and Natural Science Foundation of Fujian Province of China (No. 2015J01063).

1.T. Sparks, L. Ghadbeigi, J. K. Harada and B. Lettiere, *Energy Environ. Sci.*, 2015, **8**, 1640-1650.
2.S.-W. Kim, D.-H. Seo, X. Ma, G. Ceder and K. Kang, *Adv Energy Mater*, 2012, **2**, 710-721.
3.V. Aravindan, J. Gnanaraj, Y.-S. Lee and S. Madhavi, *Chem Rev*, 2014, **114**, 11619-11635.
4.N. Yabuuchi, K. Kubota, M. Dahbi and S. Komaba, *Chem Rev*, 2014, 11636-11682.
5.D. Kundu, E. Talaie, V. Duffort and L. F. Nazar, *Angew Chem Int Edit*, 2015, **54**, 3431-3448.
6.M. S. Islam and C. A. J. Fisher, *Chem Soc Rev*, 2013, **43**, 185-204.
7.V. Palomares, P. Serras, I. Villaluenga, K. B. Hueso, J. Carretero-González and T. Rojo, *Energ Environ Sci*, 2012, **5**, 5884-5901.
8.C. Masquelier and L. Croguennec, *Chem Rev*, 2013, **113**, 6552-6591.
9.M. H. Han, E. Gonzalo, G. Singh and T. Rojo, *Energ Environ Sci*, 2014, **8**, 81-102.
10.I. Hasa, D. Buchholz, S. Passerini, B. Scrosati and J. Hassoun, *Adv Energy Mater*, 2014, **4**, n/a.
11.D. Kim, S.-H. Kang, M. Slater, S. Rood, J. T. Vaughey, N. Karan, M. Balasubramanian and C. S. Johnson, *Adv Energy Mater*, 2011, **1**, 333-336.
12.D. Su, C. Wang, H.-j. Ahn and G. Wang, *Chem-eur J*, 2013, **19**, 10884-10889.
13.Q. Wang, B. Zhao, S. Zhang, X. Gao and C. Deng, *J Mater Chem A*, 2015, **3**, 7732-7740.
14.C. Deng, S. Zhang and Y. Wu, *Nanoscale*, 2015, **7**, 487-491.
15.H. Kabbour, D. Coillot, M. Colmont, C. Masquelier and O. Mentré, *J Am Chem Soc*, 2011, **133**, 11900-11903.
16.A. Moretti, F. Maroni, I. Osada, F. Nobili and S. Passerini, *Chemeletrochem*, 2015, **2**, 529-537.
17.S. Komaba, T. Mikumo, N. Yabuuchi, A. Ogata, H. Yoshida and Y. Yamada, *J Electrochem Soc*, 2010, **157**, A60-A65.
18.N. Yabuuchi and S. Komaba, *Sci Technol Adv Mat*, 2014, **15**, 043501.
19.J. F. Whitacre, A. Tevar and S. Sharma, *Electrochem Commun*, 2010, **12**, 463-466.
20.L. Zhao, J. Ni, H. Wang and L. Gao, *RSC Adv*, 2013, **3**, 6650-6655.
21.C.-H. Wang, Y.-W. Yeh, N. Wongittharom, Y.-C. Wang, C.-J. Tseng, S.-W. Lee, W.-S. Chang and J.-K. Chang, *J. Power Sources*, 2015, **274**, 1016-1023.
22.F. Sauvage, L. Laffont, J. M. Tarascon and E. Baudrin, *Inorg Chem*, 2007, **46**, 3289-3294.
23.H. Kim, D. J. Kim, D.-H. Seo, M. S. Yeom, K. Kang, D. K. Kim and Y. Jung, *Chem Mater*, 2012, **24**, 1205-1211.
24.D. J. Kim, R. Ponraj, A. G. Kannan, H.-W. Lee, R. Fathi, R. Ruffo, C. M. Mari and D. K. Kim, *J. Power Sources*, 2013, **244**, 758-763.
25.S. Guo, H. Yu, D. Liu, W. Tian, X. Liu, N. Hanada, M. Ishida and H. Zhou, *Chem Commun*, 2014, **50**, 7998-8001.
26.Y. Cao, L. Xiao, W. Wang, D. Choi, Z. Nie, J. Yu, L. V. Saraf, Z. Yang and J. Liu, *Adv Mater*, 2011, **23**, 3155-3160.
27.K. Dai, J. Mao, X. Song, V. Battaglia and G. Liu, *J. Power Sources*, 2015, **285**, 161-168.
28.P. Zhan, S. Wang, Y. Yuan, K. Jiao and S. Jiao, *J Electrochem Soc*, 2015, **162**, A1028-A1032.
29.H. Zheng, C. Feng, S.-J. Kim, S. Yin, H. Wu, S. Wang and S. Li, *Electrochim. Acta*, 2013, **88**, 225-230.
30.C. Zhang, C. Feng, P. Zhang, Z. Guo, Z. Chen, S. Li and H. Liu, *RSC Adv*, 2012, **2**, 1643-1649.
31.Q. Xia, X. Zhao, M. Xu, Z. Ding, J. Liu, L. Chen, D. G. Ivey and W. Wei, *J Mater Chem A*, 2015, **3**, 3995-4003.
32.F. Wu, N. Li, Y. Su, L. Zhang, L. Bao, J. Wang, L. Chen, Y. Zheng, L. Dai, J. Peng and S. Chen, *Nano Lett*, 2014, **14**, 3550-3555.
33.C. Liu, Z. Wang, C. Shi, E. Liu, C. He and N. Zhao, *ACS Appl Mat Interfaces*, 2014, **6**, 8363-8368.
34.J. Akimoto, H. Hayakawa, N. Kijima, J. Awaka and F. Funabiki, *Solid State Phenom*, 2011, **170**, 198-202.
35.W. K. Pang, V. K. Peterson, N. Sharma, C. Zhang and Z. Guo, *J Phys Chem C*, 2014, **118**, 3976-3983.
36.Q. Chu, X. Wang, Q. Li and X. Liu, *Acta Crystallogr, Sect C: Cryst Struct Commun.*, 2011, **67**, i10-i12.
37.M. Doeff, *J. Power Sources*, 2002, **112**, 294-297.
38.Q. Li, G. Li, C. Fu, D. Luo, J. Fan and L. Li, *ACS Appl Mat Interfaces*, 2014, **6**, 10330-10341.
39.M. G. Verde, H. Liu, K. J. Carroll, L. Baggetto, G. M. Veith and Y. S. Meng, *ACS Appl Mat Interfaces*, 2014, **6**, 18868-18877.
40.B. Yan, J. Liu, B. Song, P. Xiao and L. Lu, *Sci Rep*, 2013, **3**: 3332.
41.J. Li, S. Xiong, Y. Liu, Z. Ju and Y. Qian, *Nano Energy*, 2013, **2**, 1249-1260.
42.J. Hou, Y. Li, L. Liu, L. Ren and X. Zhao, *J Mater Chem A*, 2013, **1**, 6736-6741.

43.J. Liu, M. Hou, J. Yi, S. Guo, C. Wang and Y. Xia, *Energ Environ Sci*, 2014, **7**, 705-714.
44.R. Berthelot, D. Carlier and C. Delmas, *Nat Mater*, 2010, **10**, 74-80.

Graphic Abstract

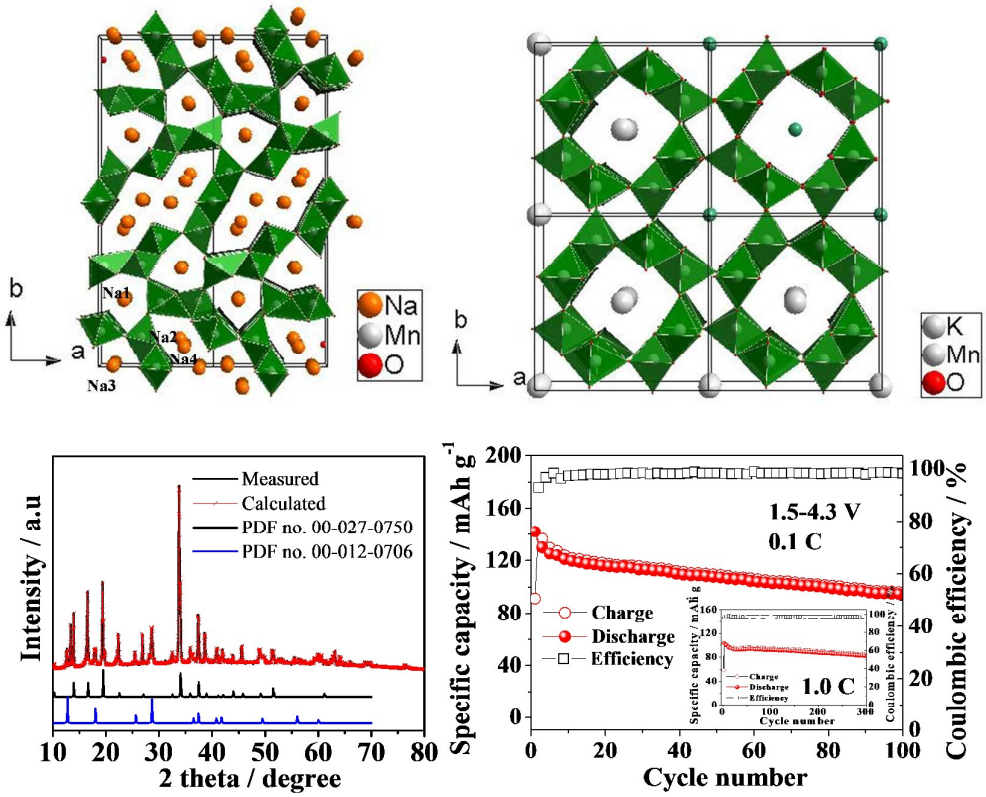

A novel tunnel $Na_{0.5}K_{0.1}MnO_2$ rod-like composite assembled by two different tunnel structures of $Na_{0.44}MnO_2$ and KMn_8O_{16} is synthesized by co-precipitation method. When used as cathode of sodium ion batteries, the composite displays outstanding electrochemical performances, which could be attributed to the combined tunnel structures, one-dimensional rod-like morphology and massive structural stacking faults.